Final Report (4/05-3/09) for NSF Project: Collaborative Research: Enabling Technology for MIMO Systems on Mobile Devices: Antennas, Switches and Packaging

Participants

During the reporting period the following people worked on the NSF project:

1) Nickolas Kingsley, Ph.D. student at Georgia Tech
2) Matt Morton, Ph.D. student at Georgia Tech
3) David Chung, Ph.D. student at Georgia Tech
4) Arnaud Amadjikpe, Ph.D. student at Georgia Tech
5) Swapan Bhattacharya, Post-Doctoral Fellow at Georgia Tech
6) Dr. Dimitris Anagnostou, Post-Doctoral Fellow at Georgia Tech
7) Dr. John Papapolymerou (PI), Georgia Tech

The PI and his students collaborated closely with the group of Prof. Jennifer Bernhard at the University of Illinois at Urbana Champaign for the design of some novel reconfigurable spiral antennas on organic substrates. We also built on our prior expertise on Sierpinski gasket reconfigurable antennas to develop some novel ones on Liquid Crystal Polymer (LCP) substrates.

Research Activities

During this project the research focused on the following topics: a) the development of a MEMS reconfigurable Sierpinski antenna on LCP substrate; b) the development of a low cost localized packaging technique for RF MEMS switches integrated on a multilayer organic substrate (this is extremely important for the switch reliability that will be required in the reconfigurable antenna system); c) the development of reconfigurable spiral antennas on organic substrate; d) moisture lifetime testing of RF MEMS switches packaged on organic LCP substrate; and e) the development of a high gain conformal antenna on LCP substrate for 60 GHz applications.

A. RF MEMS Reconfigurable Antenna

A.1. Introduction

RF MEMS switches are quickly becoming a popular switching element among microwave designers. Their low-loss, small size, excellent isolation, and low-distortion make them attractive for a wide range of applications. They have already been integrated into filters [1], antennas [2], phase shifters [3], and many other RF devices. Designers typically optimize the MEMS geometry to meet a given specification. Switches can be made wide and short or narrow and long to meet a specific size requirement. The materials can be tailored to meet a desired actuation voltage. The height of the membrane can be tuned to give a certain level of "OFF" state isolation. The inductive and capacitive regions can be designed to work best at a given frequency. For each application, there is typically one switch geometry and it is used exclusively throughout the system.

However, using only one switch geometry can be limiting if the device needs maximum reconfigurability. It could be beneficial to utilize multiple switch geometries to add an additional level of reconfigurability. For example, to provide the lowest possible loss from the switching element, several different switches could be used in parallel that are tuned for different operating frequencies. As the frequency is changed, the switch that works best at that frequency is used. This same technique could be used to select switches of different impedances, switching speed, isolation, capacitance, etc.

A system could also select between ohmic and capacitive switches to operate from DC to very high frequencies. This technique is ideal for applications that need maximum reconfigurability and can tolerate the slight size increase from the additional switches.

In this project, the use of multiple switches with different actuation voltages in the same device is investigated. RF MEMS switches are used to sequentially activate and deactivate parts of a CPW-fed Sierpinski gasket monopole antenna. The antenna has inherent multiband performance due to its resemblance to a 3-iteration Sierpinski gasket-type radiating element [4]. Since all of the switches share a common DC feed, this technique provides reconfigurability without the need for additional bias lines. This is advantageous since DC bias lines take up space, add loss, and can reduce the bandwidth of a device. This technology is particularly useful for antennas where bias lines can have a pronounced effect on radiation patterns. In this report, simulation and measurement results are presented. Some examples of possible applications are also given.

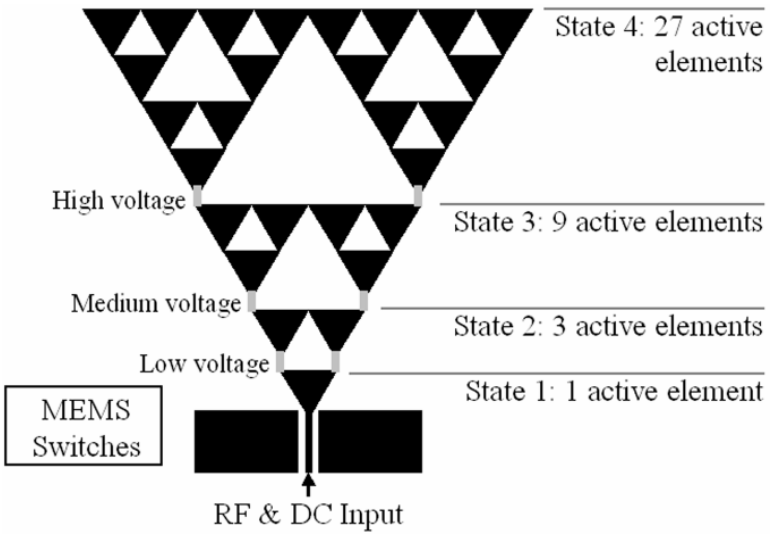

Fig. 1. Illustration of a MEMS reconfigurable Sierpinski antenna. The center line of the CPW feed provides the RF input and DC voltage for MEMS switch actuation.

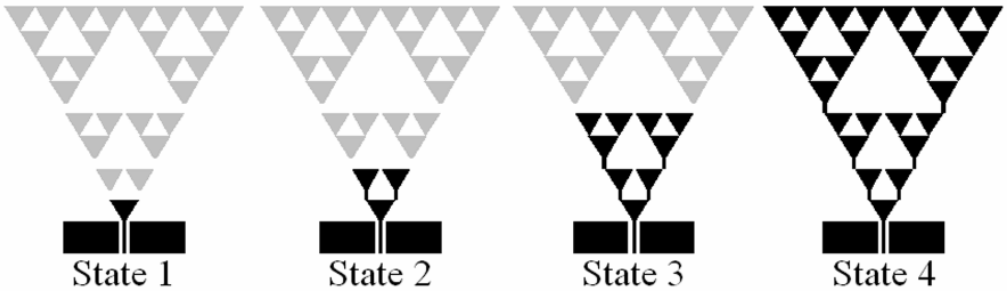

Fig. 2. The four different reconfigurable antenna states: State 1 has no voltage applied, State 2 has a low voltage applied, State 3 has a medium voltage applied, and State 4 has a high voltage applied. The activated (radiating) part of the antenna is darkened.

A.2 Implementation of Reconfigurability

The implementation of a sequentially-activated antenna is shown in Figure 1. All of the MEMS switches used are single-supported (cantilever-type) and ohmic. Regardless of the applied voltage, the triangular element that is closest to the RF/DC input is always active (Figure 2, State 1). When no DC voltage is applied, the antenna radiates at its highest frequency. When a low DC voltage is applied to the signal line, the first set of MEMS switches actuate and this activates the second level of triangular elements (Figure 2, State 2). The antenna now radiates at a lower frequency. Since all of the switches are ohmic, the low voltage is also present at the membrane of the next set of switches. However, these switches are designed to actuate at a higher voltage so they are unaffected by the voltage present. When a higher DC voltage is applied, the first set of MEMS switches remain "ON" while the second set of switches actuate (Figure 2, State 3). This activates the next iteration, consisting of six additional radiating elements. Again, this higher voltage is present at the next set of switch membranes, but the electrostatic force created is not sufficient for actuation. Finally, when the voltage is increased to its highest value, the first two sets of switches remain "ON" while the remaining set of switches actuates (Figure 2, State 4). In a way, the voltage cascades from one state to the next like a sequence of overflowing buckets. This technique could not be used if the switches were capacitive since they do not pass DC voltage. The four different states are illustrated in Figure 2, where all of the activated regions for different voltages are dark in color. This biasing technique allows for direct actuation of the electrostatic MEMS switches without the need for DC bias lines. The reduction or elimination of bias lines is highly advantageous because they can significantly distort the radiation patterns and they can introduce additional unwanted resonances.

A.3 RF MEMS Switch Design Procedure

To change the actuation voltage of a MEMS switch, there are four parameters that can be changed:

1. Membrane material: Switch membranes are almost always made of metal. This is due to their pliable nature. Stiffer metals (that is, those with a high Young's Modulus, E) will have a higher actuation voltage than those with a lower Young's Modulus.
2. Bridge thickness: The thicker the bridge, the stiffer the membrane. This gives a higher actuation voltage.
3. Bridge height: The higher the bridge, the larger the gap between the metal layers. This decreases the electrostatic force and increases the actuation voltage.
4. Membrane geometry: Springs can be designed into the shape of the membrane to lower the actuation voltage.

Of these parameters, only the fourth one does not require any fabrication changes. Making changes to a fabrication process can be a costly endeavor and may add additional variables. For example, it can be more challenging to precisely control the membrane height or thickness. For these reasons, we chose to alter the membrane geometry. By carefully controlling the spring constant (κ) of the switch, the actuation voltage can be tailored to a desired value. An example of switches with varying spring constants is shown in Figure 3.

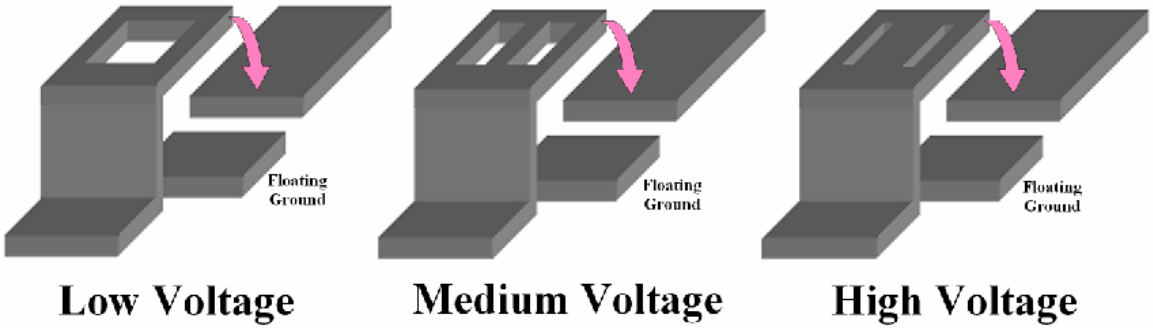

Fig. 3. Examples of ohmic MEMS switch geometries. Low voltage switches have a lower spring constant than high voltage switches. The floating ground pad is covered by a thin layer of dielectric (not shown).

A.4 RF MEMS Switch Design and Simulation Results

An accurate method for determining the actuation voltage for a given switch geometry was published in [5]. In this method, a switch is simulated using the static structural mechanics module from FEMLAB 3.0 [6]. FEMLAB, by Comsol, is a multiphysics simulator that uses the Finite Element Method. Any mechanical simulator that can perform a force-deflection analysis can use this method. Once the geometry and material specifications have been loaded into the software, a force can be applied to the beam over the electrostatic area and the deflection can be determined. The force is changed until the deflection matches the desired bridge height. This procedure is demonstrated in Figure 4.

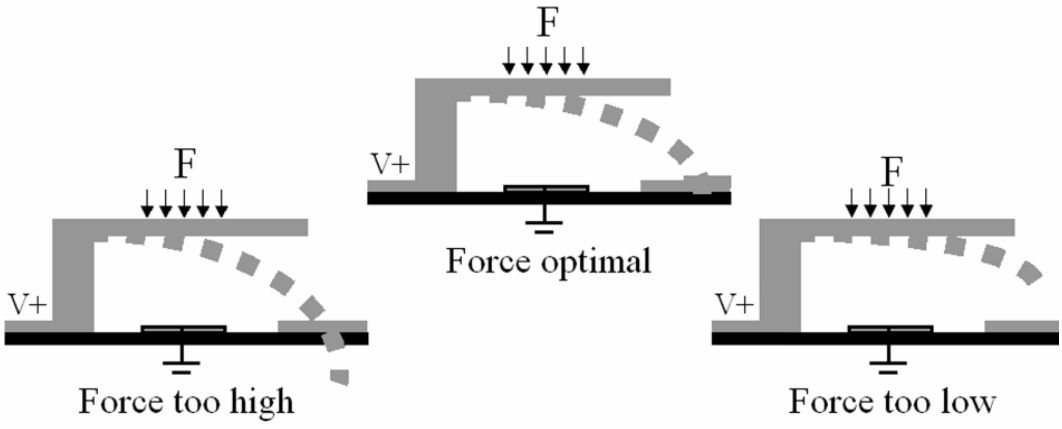

Fig. 4. Procedure for determining the optimal force needed to deflect the switch membrane. If the force is too high, the deflection is more than the membrane height. If the force is too low, the deflection does not reach the substrate. The optimal force is determined when the deflection matches the membrane height.

The actuation voltage, V, can then be calculated using:

$$V = \sqrt{\frac{2g^2F}{\varepsilon}}$$

where g is the gap (membrane height), F is the force per area, and ε is the free-space permittivity. In [5], the measured voltage was within 5V of the expected voltage.

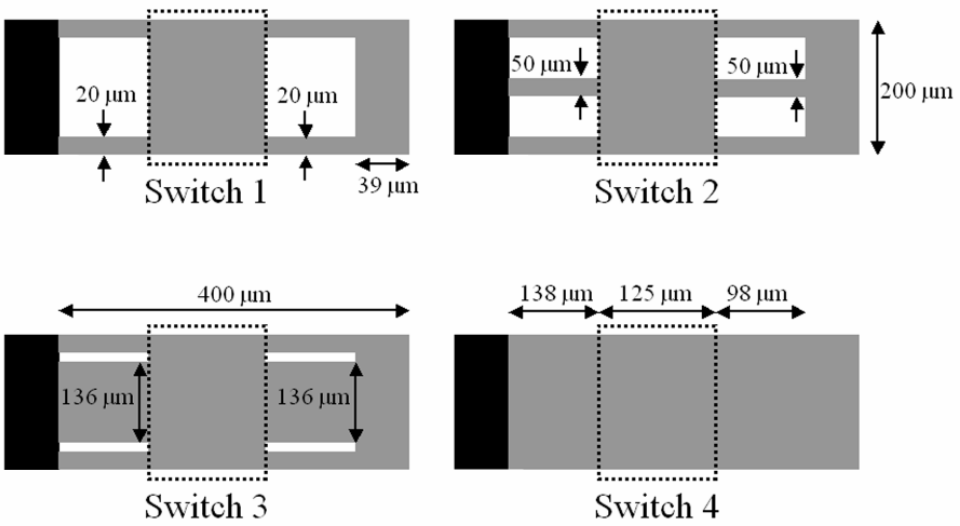

Fig. 5. A variety of switch geometries are shown. The stationary posts are shown in black. The dotted areas show the electrostatic regions. The switches are listed from lowest actuation voltage (lowest spring constant) to the highest actuation voltage (highest spring constant).All dimensions are labeled.

A.5 Mechanical Simulation Results

For the mechanical simulations, it was assumed that an aluminum bridge was used with a thickness of 2µm that was suspended 5.0µm above the substrate. Aluminum has a Young's Modulus (E) of 70 GPa, a Poisson's Ratio (η) of 0.33, and a density (ρ) of 2700 kg/m^3. Single-supported (cantilever), ohmic switches were chosen although this technique could be used with other topologies. The switch geometries shown in Figure 5 were loaded into FEMLAB with the mechanical and material properties stated before. These geometries were chosen because they have a wide variety of spring constants. They were also tuned to give a convenient ratio to the Switch 1 actuation voltage.

The simulated force that resulted in a 5µm deflection for each of the geometries is given in Table I. The deflection is shown in Figure 6. These values were entered into Equation 1 to calculate the pull-down voltage. These values are also given in Table I.

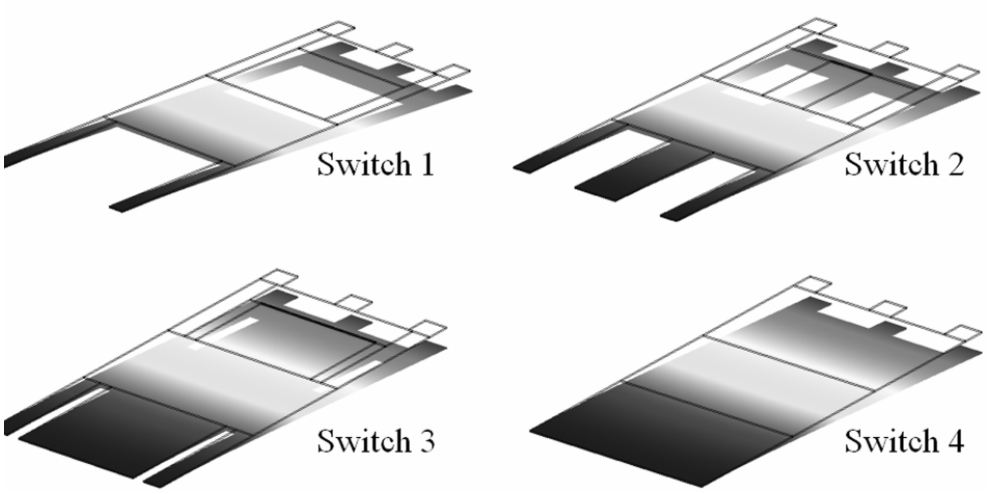

Fig. 6. The simulated deflections for the switch geometries from Figure 5 are shown. The darkest areas represent the location of the posts where there is no deflection.

Table I
Simulated pull-down force and the calculated pull-down voltage from Equation 1

Switch	Simulated Force (F)	Calculated Voltage (V)	Vswitch/Vswitch 1
1	53.90 N/m^2	17.45	1
2	121.45 N/m^2	26.19	1.5
3	236.46 N/m^2	36.54	2
4	272.21 N/m^2	39.21	2.25

A.6 RF MEMS Switch Measurement Results

The switches pictured in Figures 5 and 6 were fabricated on liquid crystal polymer (LCP) substrate. However, this technique would work for any substrate. The fabricated switches are shown in Figure 7. They all have an "ON" state resistance of about 1.7 ohms and an "OFF" state capacitance of approximately 35 fF.

The minimum voltage was measured by starting at 0V and increasing by 2V every second. This increment was chosen because it is important to actuate the switch before substantial dielectric charging occurs. When the switch actuated, S-parameter measurements were taken. These results are shown in Figures 8 and 9. The measured pull-down voltages agreed well with the expected values. These results are given in Table II.

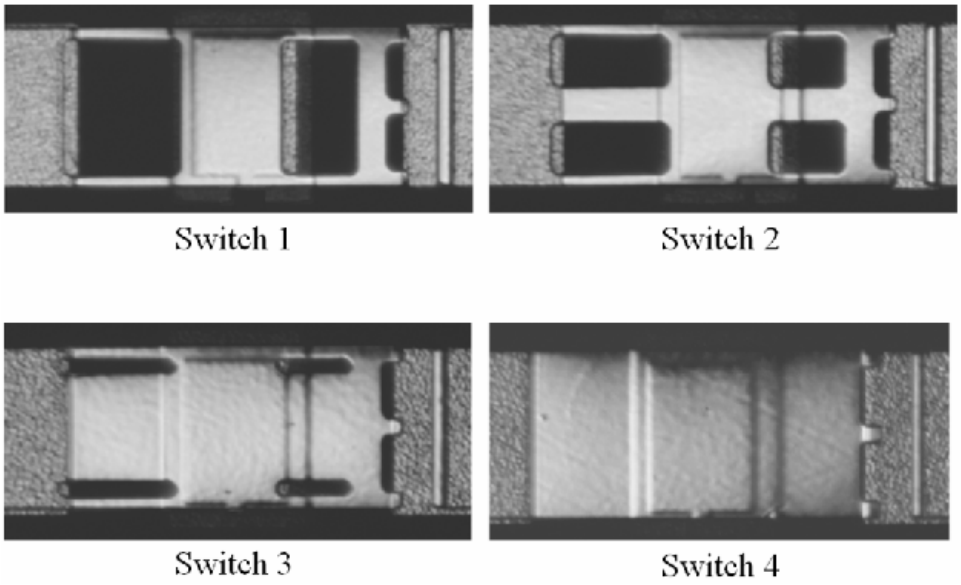

Fig. 7. Fabricated MEMS switches modeled after the designs shown in Figures 5 and 6.

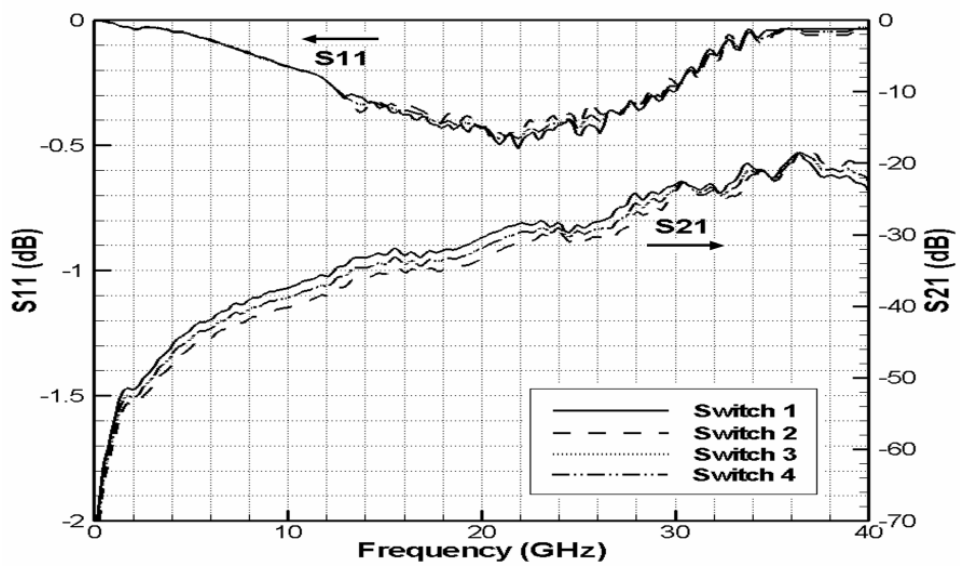

Fig. 8. S-parameter measurements results when the switch is up (not actuated).

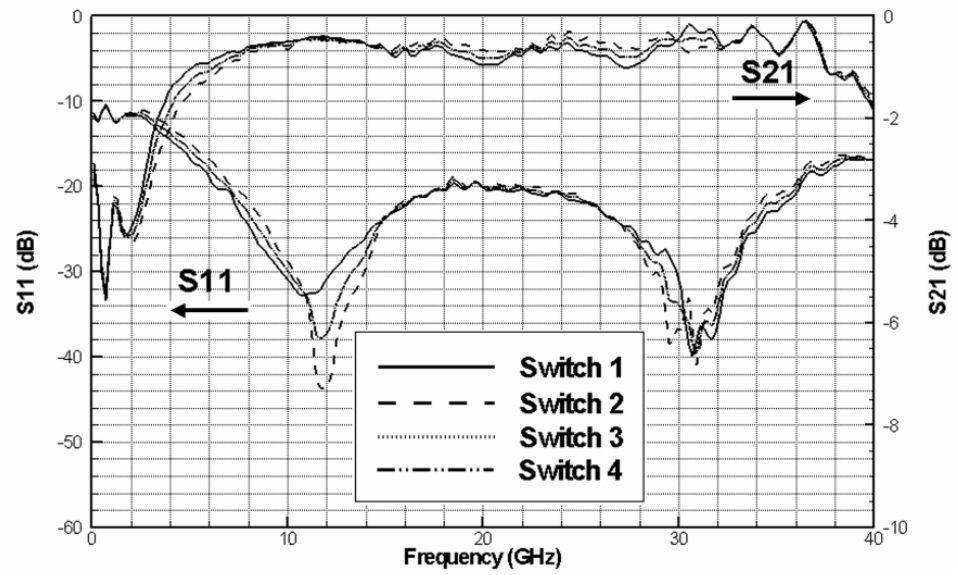

Fig. 9. S-parameter measurements results when the switch is down (actuated).

Table II
Comparison of calculated and measured pull-down voltages.
All measured voltages are within 2V of the actual minimum value due to the 2V increment.

Switch	Calculated V	Measured V	Difference	Percent Error
1	17.45 V	18 V	0.55 V	3.15%
2	26.19 V	28 V	1.81 V	6.91%
3	36.54 V	38 V	1.46 V	4.00%
4	39.21 V	42 V	2.79 V	7.12%

A.7 Antenna Design Procedure

To date, Sierpinski gasket antennas have been fabricated on many different, rigid substrates with low-permittivity (such as CuClad) and high-permittivity (such as silicon). LCP was chosen as the substrate for its numerous advantages. LCP is a thin (100μm), flexible, low-loss (tan $\delta \approx 0.004$), low moisture absorbing material with low-permittivity ($\varepsilon_r \approx 3$) [7]. Since the material is a polymer, there are additional packaging and cost advantages. All of these characteristics make it an ideal substrate for antennas, particularly at high frequencies. With respect to the geometry, the antenna elements have a 60^o flare angle and maintain the resonant structure's self-similarity with a log-periodicity of $\delta = 2$. The antenna is fed through a 6mm long CPW transmission line with a 50μm gap, a 1.3mm signal conductor width, and a 3μm thick gold layer. A picture of the fabricated antenna is shown in Figure 10. The overall size of the antenna, including the feed, is 20mm x 25mm.

The coplanar waveguide feed was chosen to facilitate the measurement setup. This reconfigurable antenna operates at four different principle frequencies. For each of these frequencies, the antenna maintains its multiband performance.

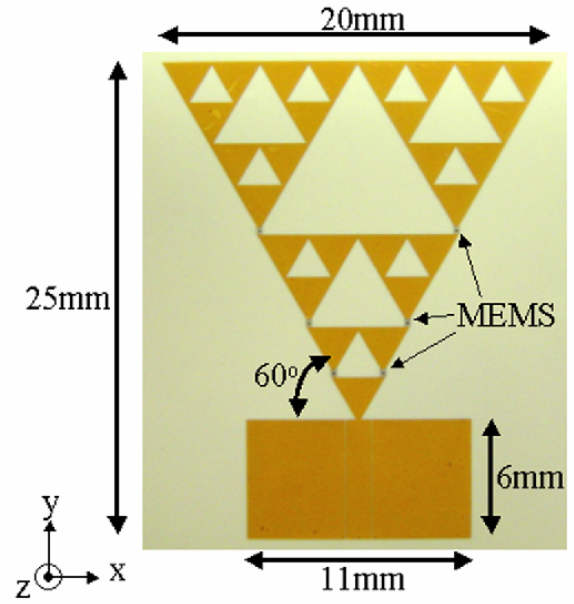

Fig. 10. Photo of the fabricated Sierpinski antenna with MEMS switches shown. The design parameters are labeled on the plot.

The antenna was simulated using IE3D [8], a Method of Moments electromagnetic solver. The simulated return loss is shown in Figure 11. The switches were modeled in two ways. First, they were simplified to a 200µm x 400µm gap in the "OFF" state and by a metal pad of the same size in the "ON" state. Those results were compared to a simulation that included the MEMS geometry in the "OFF" and "ON" states. The difference in the results between the two simulations was minor which indicates that the isolation provided by the MEMS was adequate.

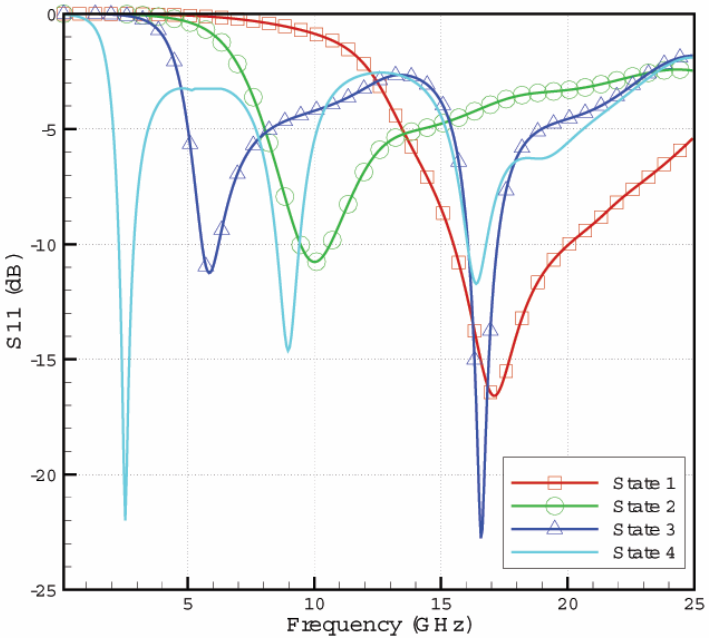

Fig. 11. Simulated return loss for all four states of the designed reconfigurable antenna.

It was verified that the antenna has a different first resonant frequency for each of the four states. Since the antenna is self-similar with a log-periodicity of 2, each time the antenna transitions to

the next state the frequency should be halved. That is, the resonant frequency of State 2 should be half that of State 1. The simulated zy-plane ($\varphi=90^o$) patterns for the four states are shown in Figure 12. These patterns are as expected for a monopole antenna. The simulated radiation pattern for the xz-plane ($\varphi=0^o$) is not presented for brevity since it shows an omni-directional pattern in that plane.

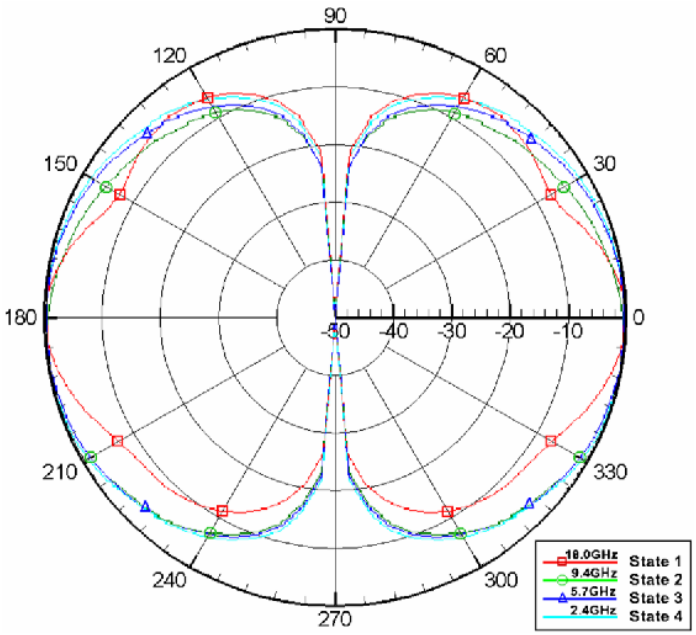

Fig. 12. Simulated radiation pattern for $\varphi=90^o$ (zy-plane) for all four states of the designed reconfigurable antenna at the first resonant frequency. It is clear that the MEMS have a minimal effect on the antenna patterns, as it maintains its broadside characteristics.

A.8 MEMS Switch Integration

The placement of the RF MEMS switches was illustrated in Figure 1 and shown in Figure 10. In order to bias the ohmic switches for electrostatic actuation, the MEMS need to have an applied voltage. A metal pad beneath the switch should be present to attract the charged metal. The metal pad must be placed under a thin dielectric material (such as silicon nitride) to prevent direct metal bridge to metal pad contact. Otherwise, no charge will develop and the switch will not actuate. This pad was shown in Figure 3. In this case, the pad is not connected to anything and is considered a floating ground. Traditionally, the actuation voltage is applied via a DC bias line. However, in order to prevent RF leakage into the DC path, careful attention needs to be given to the DC bias lines themselves. This can be implemented in different ways:

a) By using a quarter-wavelength transmission line connected to a quarter-wavelength open-circuit radial stub. Alternatively, a half-wavelength transmission line without a radial stub can be used with a reduced bandwidth. Each MEMS switch would require a different DC bias line and for this antenna that would require six lengthy metal lines being added. This would have a pronounced effect on the antenna performance. Therefore, this solution is not advisable.

b) High-resistance lines have been investigated to provide a wider bandwidth alternative [9]. Aluminum doped Zinc Oxide (AZO) is one such example, used for biasing in [10]. Thin-films of this kind are generally deposited using Combustion Chemical Vapor Deposition (CCVD), which uses very high temperatures. This is not a problem for materials like silicon, but it is much higher than the

melting point of the organic substrate (≈315°C) used in this work. At the moment, very high resistivity materials that can be deposited at low temperature are not widely available but are under investigation [11].

The proposed alternative to these approaches is to eliminate the need for DC bias lines. Instead, the biasing is handled through the antenna structure itself. Here, the DC voltage and the RF signal are both applied to the antenna through the same signal conductor of the CPW feed line. The antenna reconfigurability is made possible by using MEMS switches of varying actuation voltages.

A.9 Reconfigurable Sierpinski Antenna Testing and Results

The antenna reconfigurability was tested by varying the voltage and witnessing the antenna transition between the different states. The antenna was able to transition from the first to the last state and back again without a change in the performance. This procedure was repeated many times without problems. This demonstrates that the floating ground is sufficient.

The return loss measurements were taken with an Agilent 8510C vector network analyzer using 850µm pitch GSG RF probes. Pattern measurements were taken using an Agilent 8530 vector network analyzer with the antenna inside an anechoic chamber. End-launch gold SMA connectors were hand-soldered onto the antenna for pattern measurements. These connectors have a maximum operating frequency of 18GHz, which coincides with the highest principle frequency of the antenna when no voltage is applied. Since the gap in the CPW lines is 50µm wide to achieve 50Ω for our chosen signal line width, manual soldering of the connector pin may not always result in a smooth transition. This can cause undesired ripple in the measurements at higher frequencies. The return loss measurement results are shown in Figure 13. The resonant frequencies roughly halve as the antenna increases in size. These measurement results are summarized in Table III and agree well with the simulated values shown in Figure 11.

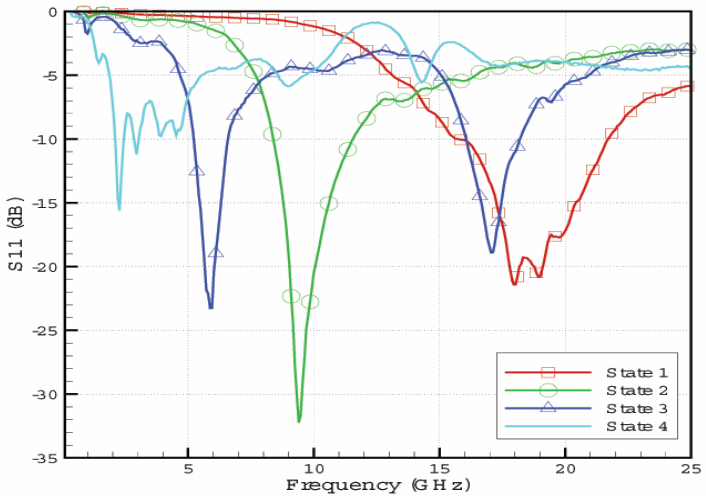

Fig. 13. Measured return loss for all four states of the designed reconfigurable antenna.

Table III
Tabulated antenna measurement results for all four states.
The actuation voltage and measured resonances are given.

State	Voltage	f_1	f_2	f_3
1	0 V	18.0 GHz	> 30 GHz	> 30 GHz
2	18 V	9.4 GHz	> 30 GHz	> 30 GHz
3	28 V	5.7 GHz	17.5 GHz	> 30 GHz
4	38 V	2.4 GHz	9.0 GHz	14.3 GHz

The measured normalized patterns are shown in Figure 14. Some ripple can be noticed in State 1 of the antenna due to mismatch from the coaxial SMA connector. The measured patterns agree well with the simulated ones shown in Figure 12. For clarity, these plots are not superimposed. The measured radiation pattern for the xz-plane ($\varphi=0^o$) is not presented as before since it shows an omni-directional pattern in that plane.

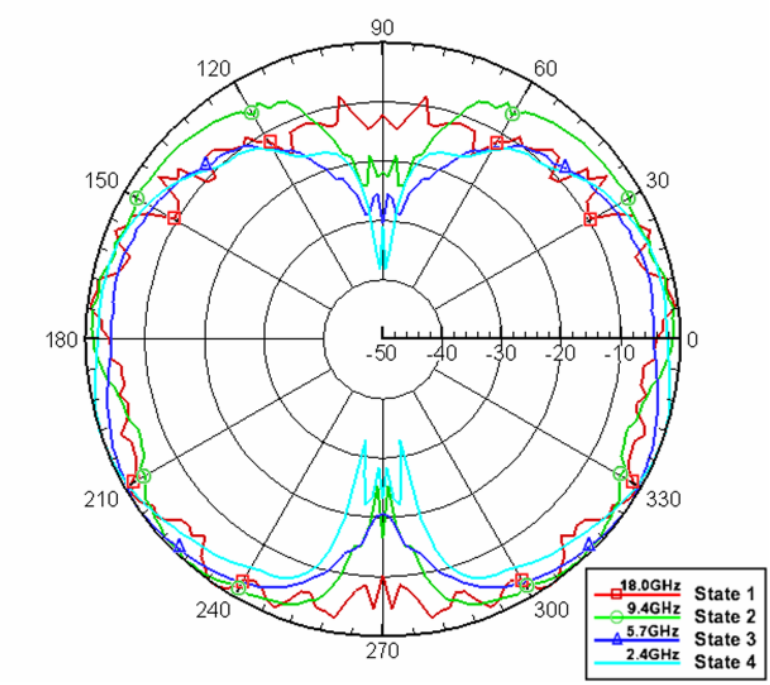

Fig. 14. Measured radiation pattern for $\varphi=90^o$ (zy-plane) for all four states of the designed Reconfigurable antenna at the first resonant frequency. Broadside radiation with similar patterns at each frequency is achieved. The different curves at 2.4GHz, 5.7GHz, 9.4GHz, and 18.0GHz validate the multiband characteristics that can be achieved by using MEMS to reconfigure such antenna designs.

A.10 Conclusions

This work presents the possibility of adding an additional level of reconfigurability to a device or system by simply integrating RF MEMS switches with different geometries. A sequentially-reconfigurable RF MEMS multiband antenna was designed, fabricated and tested on a flexible, organic substrate for the first time. The purpose of this research was not only to illustrate a method of biasing MEMS-reconfigurable antennas without the need for DC bias lines, but also to illustrate how

the antenna performance can be enhanced by increasing the number of resonant frequencies. The final device does not have any additional lines to bias the switches, while the antenna exhibited four principle resonant frequencies with good radiation characteristics. By using MEMS switches, the losses are kept to a minimum. Three different switch geometries were integrated into a Sierpinski antenna with different actuation voltages. The simulated and measured response agreed well. This technology can be applied to many other devices, including tuners, tunable filters, other antenna geometries, or signal splitters.

B. Localized Packaging Technique for Organic RF MEMS Switches

B.1 Introduction

LCP has recently been shown to be an ideal material both as a substrate for high-frequency RF performance and as a packaging medium because of its very low dielectric loss, near-hermetic nature, and extremely low cost [12]. LCP has also been successfully implemented in the packaging of MEMS sensors [13], and RF MEMS switches [14], [15]. However, current packaging methods rely either on low-temperature LCP or intermetallic bonding, which require temperatures in excess of 290◦C and 260◦C respectively. While these temperatures may be acceptable for certain sensor applications, this temperature exceeds the maximum allowable temperature of popular RF MEMS switch architectures such as the capacitive membrane [16]. Above 200 C, the relatively large membrane of these switches suffers from plastic deformation, which has a permanent negative effect on the performance of the device. Additionally, recrystallization of the gold membrane becomes a factor at these temperatures, which can cause a further decrease in RF performance and reliability [17]. As such, the excellent hermeticity results from the lamination technique described in [14] require temperatures that damage the MEMS devices and degrade performance, seen as poor insertion loss and isolation in the post-bonded switch [15]. These works used the Radant ohmic contact switch, which requires 90 V due to the higher stiffness. If lower actuation voltage (20-30 V) capacitive membrane switches were packaged with the lamination method, the performance would be degraded even further. Clearly, lamination techniques are not viable for high-performance packaging of temperature sensitive devices.

Localized heating techniques have been used to package temperature-sensitive MEMS sensors using patterned aluminum lines within a stack-up of plastic layers [18], and similar methods have been demonstrated with silicon substrates [19]. This allows for high heat at the bonding regions while the device remains at a safe, much lower temperature. However, embedded metal lines would cause significant degradation in RF performance for MEMS devices. This work investigates the use of patterned lines on copper clad LCP as a low-cost method for packaging RF MEMS switches (Fig. 15). A significant advantage of this method is the use of heating lines external to the stack-up allowing for easy removal and hence no impact on RF performance as seen in previous work. Simulations of the heating element structures are performed to examine the thermal characteristics of the bonded regions and switch. Heating lines are fabricated on LCP requiring only one photolithography and etch step, and the MEMS cavity is formed with two 1 mil layers of low-temp LCP that are etched with a CO2 laser system. This laser etch is performed only to quickly etch the low-temp LCP layer into cavities for prototyping, not used in forming the seal as in some more complicated bonding methods. The layers are bonded with localized-heating by passing 7 A of DC current through the heating element while compressing the 4 layers together. The bonded switch is submerged in 60 ^{o}C water for 24 hours to test seal quality. Before and after measurements are shown, providing evidence of a successful bond. No lasers or exotic heating materials are required in the sealing process, resulting in a very low cost packaging solution. A low cost localized heating method for temperature sensitive MEMS devices on LCP using the provided copper cladding is shown for the first time.

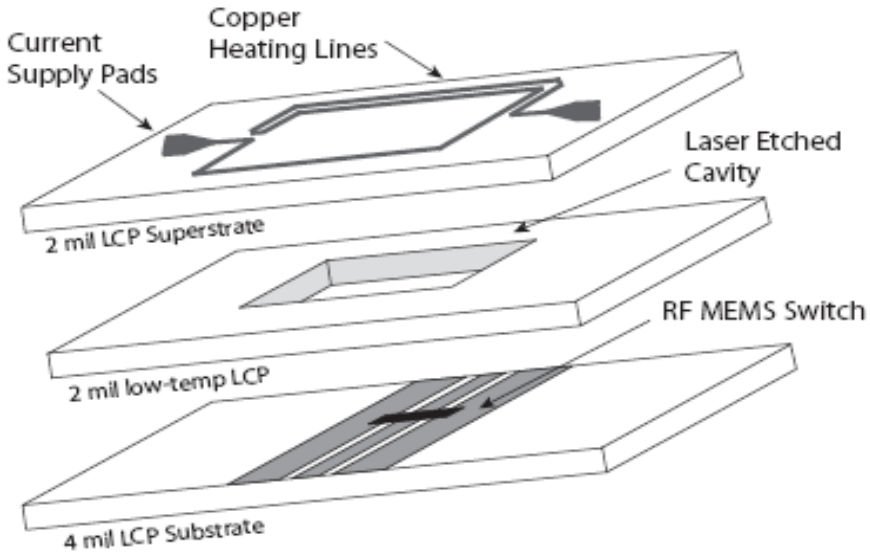

Fig. 15 Layer stack-up for localized heating method.

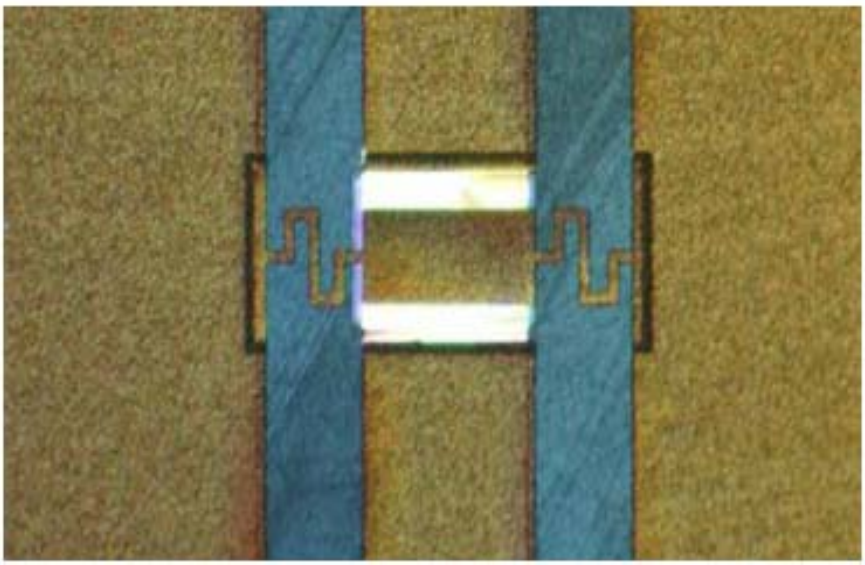

Fig. 16 Capacitive membrane MEMS switch used in the bonding process.

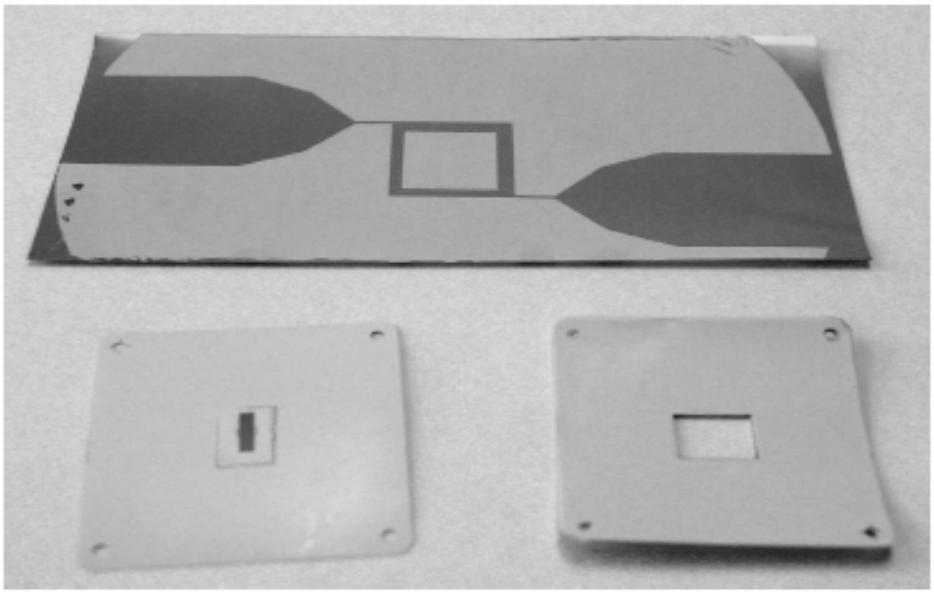

Fig. 17. Photograph of heating element superstrate, laser etched spacer layers and MEMS LCP substrate prior to bonding.

B.2 Implementation

A capacitive membrane MEMS switch is fabricated on 4 mil LCP using a previously published fabrication process [20]. Fig. 16 shows the fabricated switch, featuring meandered springs to reduce pull-down voltage.

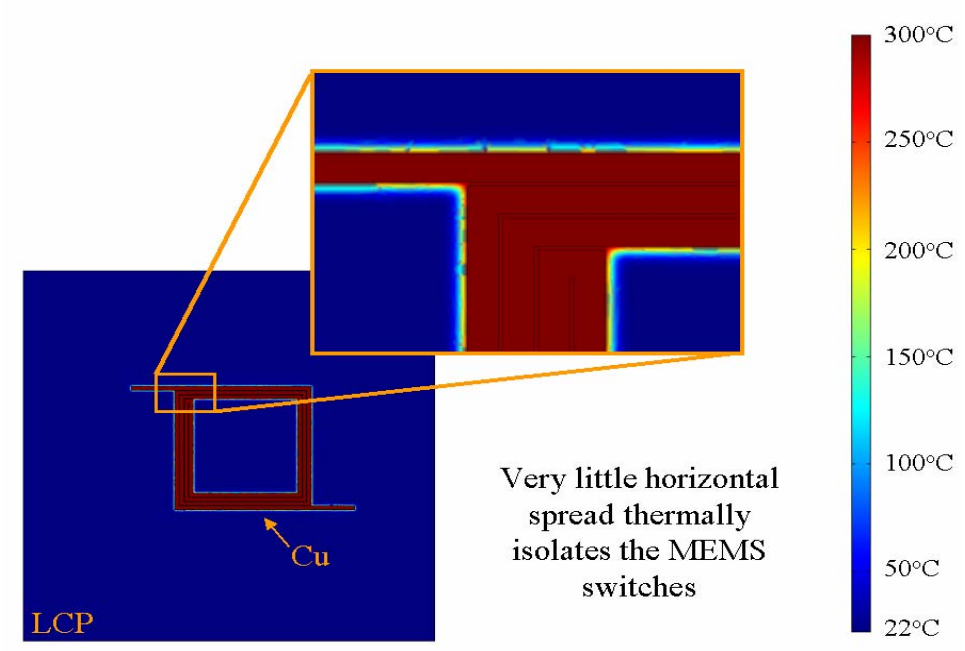

Fig. 18 Temperature distribution viewed from top of package showing lateral thermal flow through the LCP layer.

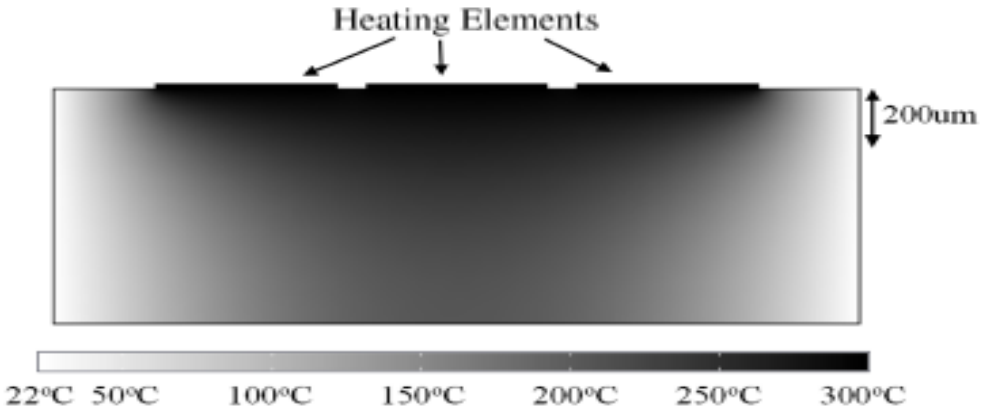

Fig. 19 Temperature distribution viewed from side of package, showing heat emanating from the three spaced heating element lines into the LCP layer.

The heating element is fabricated on copper clad 2 mil LCP (Fig. 17). 500 μm wide lines are patterned via photolithography and etched in copper etchant. The lines form a rectangular region that encircle the desired bonding area, consisting of 34 heating lines per side to facilitate a wider bonding region. The heating lines are tapered out to a large 1 inch wide line at either end. The large lines provide higher conductivity which generates significantly less heat than the 500 μm lines during bonding and allows easy access for the bonder current supply. Tapers limit excessive heating at the junctions between line widths resulting from high local resistance.

A cavity for the MEMS switch is fabricated from two pieces of 1 mil low-temp LCP. These layers are etched with a CO_2 laser system to provide room for the switch and contact the area of the heating rectangle on the heating element sample. The four layers are sandwiched together and pressed between high-temperature glass slides with enough pressure to keep the heating elements from delaminating during heating. Glass was used as it is a poor thermal conductor, which keeps heat generated at the heat elements from sinking to the slides and reducing heat flow to the internal LCP layers. 7 A of DC current is applied to the heating element, pulsed at 60 Hz for 30 seconds. Switching the current allows for better thermal transfer vertically through the layers without causing the top layer to heat excessively. Higher currents can be used for faster bond times, but this causes the heat on the top layer to potentially damage the top LCP or copper lines. The patterned heating elements reside on the topside of the heating layer, so they can be easily etched after bonding. This requires thermal transfer through the top layer, but removes impact of the copper heating lines on RF performance.

The bonding method can easily be scaled up to accommodate multiple individually packaged devices (wafer-scale packaging). Wider lines can be used between bonding regions to limit the areas where the melting temperature is reached. Expanding the bonding area or bonding additional regions simultaneously requires the same amount of current (assuming a constant heating line width is kept at the bonding regions), but higher voltage resulting from the larger resistance seen at the current supply terminals. Using thinner metal layers will result in higher resistance for the same line geometry, trading current requirements for higher voltages. Because the heating lines are patterned, complicated seal shapes and extremely varied seal sizes and geometries can be created for simultaneous bonding at wafer-scale.

B.3 Thermal Simulations

FEMLAB 3.1 multiphysics simulator by COMSOL [21] was used to simulate the ring bonding environment. The steady-state, conduction, heat transfer module was used to simulate the transfer of

heat to the MEMS switch. Two-dimensional simulations were performed from the top and side perspectives. The impact of the bonding process on the MEMS switch was investigated. LCP, like most polymers, is a poor thermal conductor. It is about 17 times more conductive than air while silicon is almost 300 times more conductive than LCP. This means it would take significantly more energy to heat up a sample of LCP than it would for a sample of silicon. Since we need to bond layers of LCP using heat, it is important to study how efficiently heat can spread through LCP. Since a mechanical model is being used, the appropriate physical constants must be entered for LCP. These values are shown in Table IV.

For the first simulation, the entire ring is simulated with enough room around the borders to show the lateral spread of heat. A perfect thermal insulating boundary condition is used at the extremities to provide a reference point at room temperature (22 C). The copper lines are heated to 300 C and the package is allowed to reach the steady-state. The results from this simulation are shown in Figure 18. As desired, the heat spreads very well around the copper traces but does not extend much laterally. This is desired since it is important that the high temperature does not reach the switch area.
For the second simulation, a cross section of one side of the ring is simulated with enough depth to show the vertical spread of heat. Again, a perfect thermal insulating boundary condition is used at the extremities to provide a reference point. The copper lines are heated to 300 C and the package is allowed to reach the steady-state. The results from this simulation are shown in Figure 19. This simulation further demonstrates how poorly the heat spreads laterally. Since LCP will not melt below 290 C, for copper lines heated to 300 C, there is approximately 200μm of vertical bonding. For thicker bonding layers, a higher metal temperature will be required. From these simulations, it can be concluded that metal ring bonding techniques can be used to package RF MEMS devices.

Table IV LCP properties

Property	Symbol	Value
Young's Modulus	E	16 GPa
Poisson's Ratio	ν	0.3
Density	ρ	1400 $\frac{kg}{m^3}$
Thermal Conductivity	k	0.5 $\frac{W}{mK}$
Relative Permittivity	ϵ_r	3.1

B.4 Measurements

The switch was measured from 2-40 GHz on an Agilent 8510C network analyzer with an SOLT calibration. Measurements of the switch were taken before any bonding operations took place. After bonding, the switch was submerged in 60 C water for 24 hours. After removal, the package was peeled apart without any interruption to the internal state of the cavity (i.e., no heating to remove residual moisture), and the switch was measured a second time. Before and after measurements can be seen for the up (non-actuated) state and the down (actuated) state in Figs 20 and 21 respectively. The switch exhibits 0.5–0.6 dB loss in the up state, which includes 1 cm of line loss for the CPW line. Removing line loss, the switch generates a loss of 0.2–0.3 dB up to 40 GHz. Return loss in the up state is better than 20 dB for 2-40 GHz. In the down state, the switch maintains isolation better than 20 dB for frequencies > 15 GHz. The switch was designed with a high frequency resonance to provide the highest level of RF performance at frequencies where active switches (pin diodes, FET technologies, etc) are unable to match the capability of the capacitive membrane MEMS switch. No appreciable

difference in RF performance was observed in before and after measurements, indicating that no water was introduced to the internal packaged cavity during water submersion.

To test the impact of the bonding method on RF performance, an FGC line was measured before and after bonding. The after measurements were taken with the heating lines removed post-bonding, leaving the seal intact. Fig. 22 shows very little difference between these two cases, showing the RF impact of the sealing method is negligible.

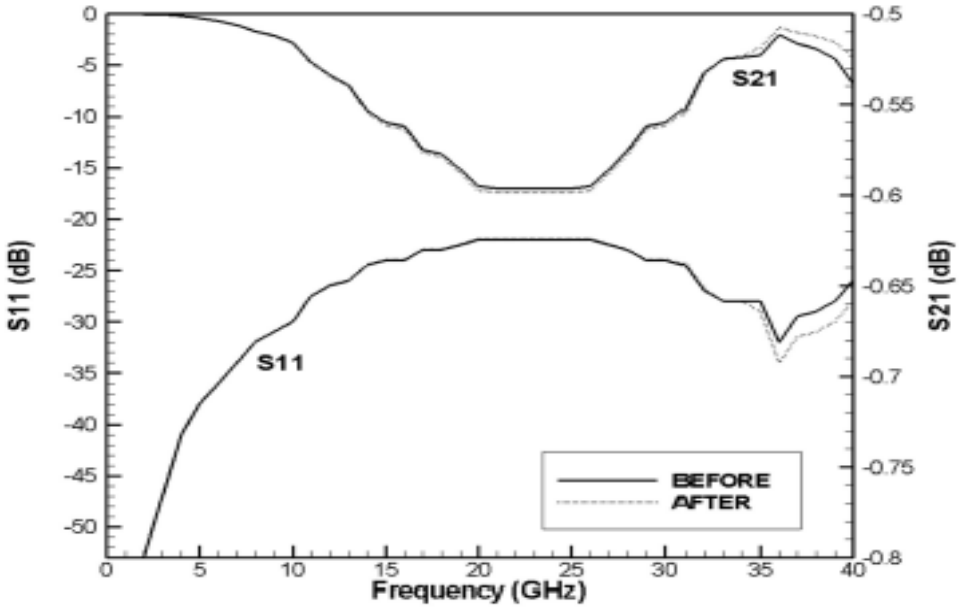

Fig. 20 Measurement results of switch before and after water testing in UP (non-actuated) state.

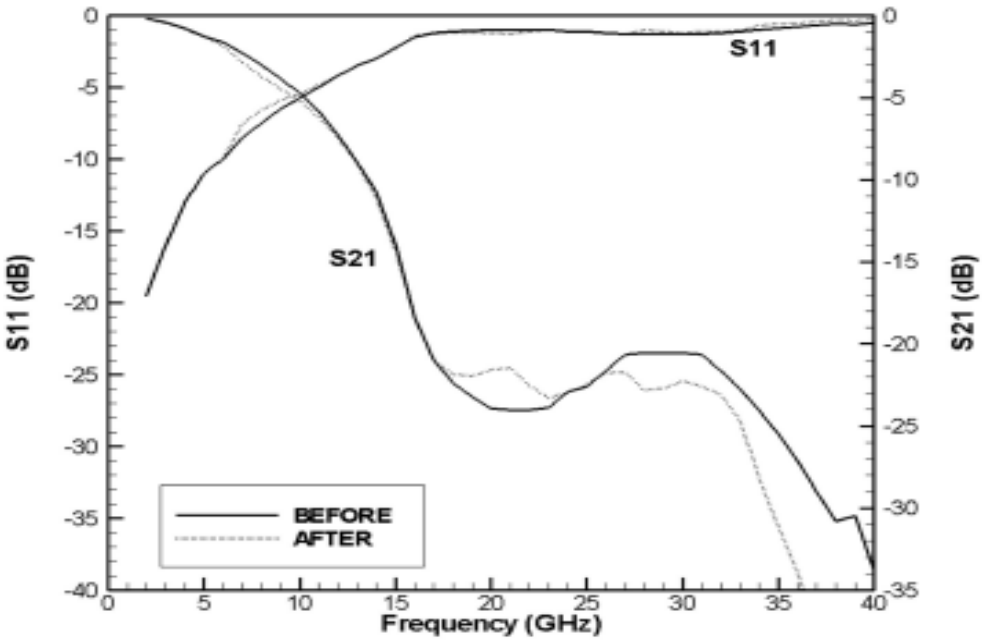

Fig. 21 Measurement results of switch before and after water testing in DOWN (actuated) state.

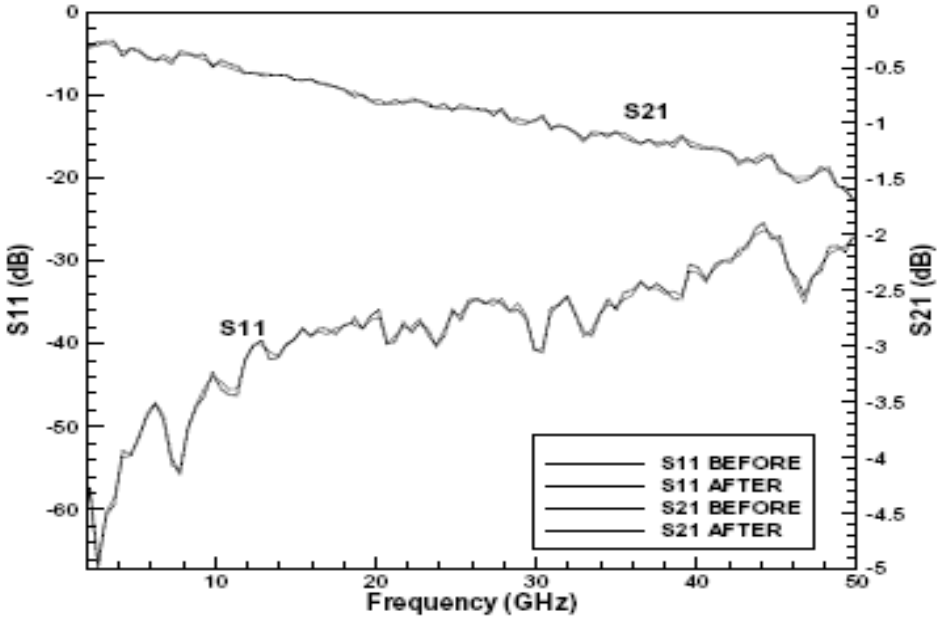

Fig. 22 Measurement results of FGC line before and after bonding with heating lines removed.

B.5 Conclusions

A low cost localized heating method for LCP using the provided copper cladding has been shown for the first time. Simulations of the heating element structures were performed to examine the thermal characteristics of the bonded regions and switch. Heating lines were fabricated on LCP requiring only one photolithography and etch step, and the MEMS cavity is formed with two 1 mil layers of low-temp LCP that were etched with a CO2 laser system. The layers were bonded with localized-heating by passing 7 A of DC current through the heating element while compressing the 4 layers together. The seal quality was tested by submerging the packaged switch in 60 C water for 24 hours. Measurements after soaking indicate the bonding technique is successful. The bonding technique can be scaled for different LCP thicknesses and seal geometries. This bonding method provides a very low cost solution to packaging temperature sensitive devices such as the capacitive membrane RF MEMS switch. Unlike previous attempts at localized heating, the easy removal of all heating line metal removes the RF degradation associated with the heating lines, leaving only high performance LCP. This eliminates the need to tailor transmission lines to widely different impedances that are seen with alternative bonding approaches. Hence, this work improves upon the method shown in [14] by packaging a MEMS device without degrading the RF performance and providing a solution that can accommodate a wide range of temperature sensitive devices. Due to the minimal impact on RF performance, ease of scalability, versatility and low cost, this bonding method is an ideal solution to packaging MEMS devices in such high-performance polymers as LCP.

C. Fabrication of Reconfigurable Antennas

The UIUC 26 GHz antenna design was fabricated on LCP substrate with the MEMS switches integrated (for more information on the antenna design please refer to the annual report submitted by Prof. Bernhard for the same project). Cantilevers with a capacitive contact were used. PECVD silicon nitride deposited at 150^{o}C was used as the dielectric. Fig. 23 shows the top view of the 9 antennas fabricated in a 3x3 configuration. The photo shows the antennas and the DC bias lines with the DC

contact pad. Several antennas were fabricated to mitigate yield issues. The antennas were sent to Illinois for drilling the via-holes for the RF ground and the micro-coaxial feed. As soon as the via drilling is completed the return loss and the radiation patterns of the antennas will be measured at Illinois. The results for this antenna will be presented in the UIUC final report.

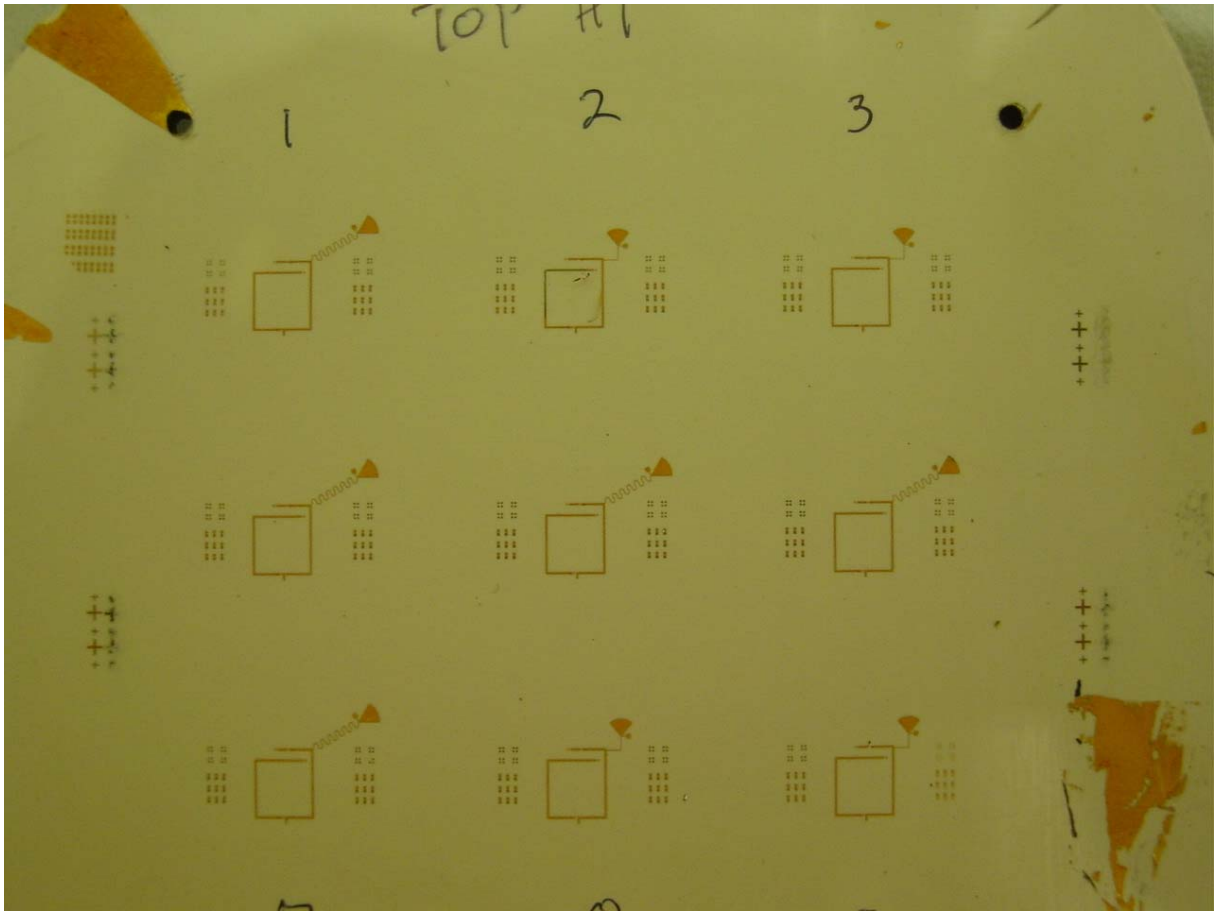

Fig. 23. Photo of fabricated reconfigurable antennas with RF MEMS switches on LCP.

D. Moisture Lifetime Testing of RF MEMS Switches Packaged in Liquid Crystal Polymer

In this work, MEMS switches were packaged in a polymer material and subjected to two humidity conditions. The polymer material chosen was liquid crystal polymer (LCP). LCP has been well-documented as a low-cost material that is also low-loss up to 110 GHz. According to the manufacturer, LCP has a "water absorption" of 0.04% . S-parameter results are shown before and after testing to determine the effects of the moisture exposure. The lifetime of an LCP packaged switch was extrapolated for jungle, ambient, and desert-like conditions.

The MEMS switches used in this work were fabricated directly on the LCP material. Single-supported, capacitive-type switches were used although the experimentation and results are applicable for ohmic and double-supported switches as well. These switches were designed to work at 30 V actuation. They are made with 1 um plated gold suspended approximately 1 um above the substrate.

The overall dimensions of the membrane are 200 um 400 um. The fabricated MEMS switch is shown in Fig. 24. Since the MEMS switches will be contained in a package entirely made of LCP, there are two possible sources of moisture: through the LCP material and through the seal. Ideally, MEMS switches would be packaged between layers of LCP using wafer-scale (or global) thermocompression bonding. However, LCP melts at 290 ^{o}C and MEMS switches experience plastic deformation above 200 ^{o}C. Therefore, it is necessary to implement the bonding process using an epoxy or a localized heating technique.

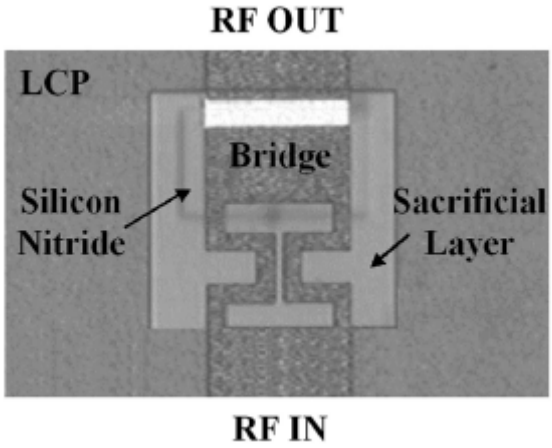

Fig. 24. Photo of fabricated MEMS switch on LCP . The sacrificial layer is removed to facilitate the suspended bridge.

Since the objective of this research is to determine the moisture resistance of LCP alone, no epoxy bonding was used. Instead, three sample configurations were investigated:

1) Global lamination with an air-filled cavity (no MEMS switch).

2) Global lamination with an air-filled cavity and 18 um thick copper on the top and bottom (no MEMS switch).

3) Localized ring bond with an air-filled cavity and MEMS switch.

These configurations are shown in Fig. 25. For Configurations 1 and 2, global thermocompression bonding was performed. For this bonding, the layers are heated to the melting temperature over the course of 10 min. They are then held under compression for 45 min. The sample is continually held under compression until it cools to room temperature. Since this process is slow, the molecules have time to arrange in the same crystal-like state as they did before melting. Even though RF MEMS switches can not survive this process, it does represent the best-case scenario that can be achieved with direct LCP to LCP bonding. Bond widths of 2, 5, and 10 mm were tested. For Configuration 3, a seal around the MEMS switch was formed using resistive heating of thin copper lines. The layers of LCP are heated under force to the molten state in less than 5 s. They are then held in place at this temperature and pressure for 30 s to ensure that uniform melting has occurred.

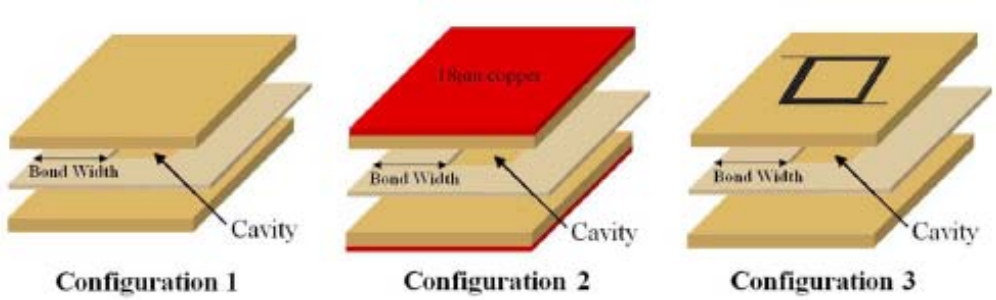

Fig. 25. Three sample configurations. A cavity is formed by bonding two layers of high-melt LCP to a layer of low-melt LCP with a hole cut in the material. The bond width dimension is shown.

While maintaining a constant pressure, the temperature is allowed to cool down to room temperature over the course of 5 min. Since the entire process is quick, the heat from the bonded areas does not affect the MEMS switches. The bond width is approximately 2 mm. To provide the best possible bond quality and consistency across samples, several precautions were taken. First, all of the samples were plasma cleaned prior to bonding to remove any trace amounts of dust, dirt, oils, or other impurities. Second, all processing was performed in a class 10 cleanroom environment. Third, all cavities are of the same size (2cm x 2cm x 50μm or 0.02 cm^3). Finally, all samples were processed at the same time in a low-humidity environment.

Before and after testing, all samples were baked for 1 h at 100 ^oC on a hot plate. This step is necessary to remove any surface moisture that will not compromise the integrity of the package but can skew the weight measurements. Precautions were taken to protect the samples from dirt and oils. All weight measurements were repeated a week after sitting in ambient conditions with identical results. It can be concluded that this dry bake temperature and duration were sufficient. All measurements were taken with a scale that has five digits of precision and is enclosed to eliminate the effects of room pressure changes. According to Military Standard 883 G, Method 1014.12, a cavity with a volume of 0.02 cm can pass the seal leak test with less than 2 mg of weight gain.

To evaluate long duration exposures to the elements (up to 10 years), a test was performed at 100 ^oC and 100% relative humidity for 1, 5, and 10 h. The measured weight gain from this test is shown in Table V. A visual inspection of the MEMS in Configuration 3 showed that the switches had been affected by moisture. Measurement results confirmed that the switches did not survive the test and were stuck in the DOWN state. In this work, only the 2 mm bond width was tested for Configuration 3. This is due to the difficulty in realizing wide bond widths using localized heating techniques. The 10 h test was not completed for this configuration since the 1 and 5 h samples leaked profusely. There are two samples that gained a great deal more moisture weight than the others (Configuration 1, 10 mm, 10 h and Configuration 2, 10 mm, 1 h). A visual inspection did not find any indication of why these samples leaked profusely. Since LCP is a polymer, defects in the material are always possible and can not be avoided.

To evaluate the short term effects of moisture, a second test was performed at 85 ^oC and 85% relative humidity. This test has roughly one-fifth the acceleration factor of the 100 ^oC/100% test and is the equivalent of about three months of ambient exposure. The weight gain from this test is shown in Table VI. All tests passed the Military Standard. The post-test S-parameter measurement results are shown in Fig. 26. The 30 min switch was able to actuate without problems at 30 V [Fig. 26(a)]. The 50 min switch had deformed enough that it was only able to move a fraction of a micron at 100 V. Only a slight change in the response was measured [Fig. 26(b)]. The 70 min switch was unable to move at all [Fig. 26(c)]. Since the 30 min switch survived the moisture exposure, a comparison can be made in the S-parameter measurements before and after testing. These results are shown in Fig. 27. This comparison confirms that there was no degradation in the performance due to the moisture exposure.

TABLE V
WEIGHT GAIN MEASURED FOR THE THREE CONFIGURATIONS AT 100 C AND 100% RELATIVE HUMIDITY. AT THIS TEMPERATURE AND HUMIDITY, 1 H OF TESTING IS EQUIVALENT OF ONE YEAR IN AMBIENT CONDITIONS

Bond Width/Duration	Config. 1	Config. 2	Config. 3
2mm/1 hour	0.3mg	0.1mg	5.5mg
2mm/5 hour	0.3mg	0.5mg	8.2mg
2mm/10 hour	0.8mg	0.2mg	Not tested
5mm/1 hour	0.4mg	0.7mg	Not tested
5mm/5 hour	0.5mg	0.2mg	Not tested
5mm/10 hour	0.4mg	0.1mg	Not tested
10mm/1 hour	0.5mg	1.5mg	Not tested
10mm/5 hour	0.6mg	0.3mg	Not tested
10mm/10 hour	6.4mg	0.3mg	Not tested

TABLE VI
WEIGHT GAIN MEASURED UNDER 85 C AND 85% RELATIVE HUMIDITY CONDITIONS. ALL SAMPLES HAVE A 2 MM BOND WIDTH

Sample	Weight Gain	Switch worked after testing?
Config. 1 - 30 minutes	0.1mg	N/A
Config. 1 - 50 minutes	0.1mg	N/A
Config. 1 - 70 minutes	0.1mg	N/A
Config. 3 - 30 minutes	0.1mg	YES
Config. 3 - 50 minutes	0.2mg	NO
Config. 3 - 70 minutes	0.2mg	NO

From the data in Table V, several conclusions can be made:

1) All packaged cavities resulted in at least 0.1 mg of weight gained.
2) The presence of the 18 um thick copper had very little effect (less than 10% improvement) on the amount of weight gained. This suggests that most of the leakage is through the seal, not the material.
3) Most of the weight gain occurs within the first hour of testing.
4) The bond width has a negligible effect on the rate or amount of weight gained
5) For some cases, as the duration is increased, the weight gain decreases. This demonstrates the inconsistency with polymer materials.
6) Of the 18 globally laminated samples in Configurations 1 and 2, only one test failed the Military Standard. Both locally bonded samples in Configuration 3 failed.

The data in Table VI supports these conclusions as well. This work has also shown that passing the Military Standard for seal quality does not guarantee that the package is suitable for MEMS switches. All of the cases shown in Table VI passed the standard but only one switch actually survived. If 0.1 mg of weight gain is the actual amount of moisture that the switch can tolerate for this cavity size, then the data in Table V suggests that even the best-case bonding effort is not suitable for reliable MEMS packaging. Sixteen of the eighteen samples gained more than 0.1 mg of moisture weight.

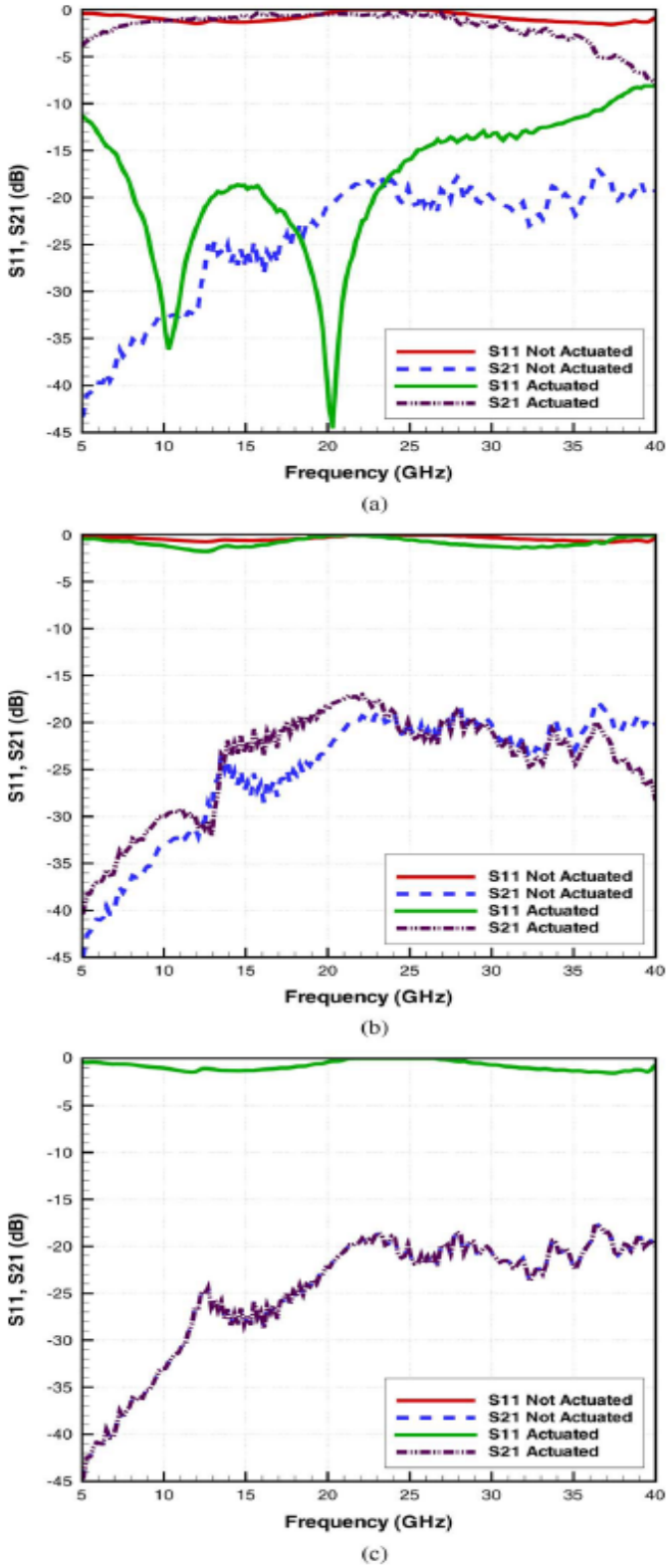

Fig. 26. S_{11} and S_{21} measurement results for the three 85 C/85% moisture test durations. Measurement 26(a) shows a working switch with a 30 V actuation. Measurement 26(b) shows a non-working switch with some movement at 100 V. Measurement 26(c) shows a switch stuck in the not actuated (UP) state.

Aside from measurement data, a visual analysis can also provide an indication of the damage that has occurred from moisture exposure. The metal bridge membrane is relatively unaffected by low levels of moisture. As the humidity level within a cavity is increased, the edges of the membrane begin to curl. Effectively, this strengthens the bridge in the axis of motion. This type of curling was seen in the switches exposed to the 85 ^{o}C/85% condition for 50 and 70 min. This is why the membrane did not actuate even at very high voltages. The curling was less severe in the 50 min sample which is why it was able to deflect slightly. Both of these samples were stuck in the UP state. As the humidity level increases further, moisture begins to collect on the metal membrane and the signal line beneath it. If the humidity level increases high enough, the surface tension in this moisture will pull the switch down. This effect was seen in the switches exposed to the 100 ^{o}C/100% condition. These switches were stuck in the DOWN state. Using the acceleration factors, it can be extrapolated that an LCP packaged MEMS switch using localized ring bonding (Configuration 3) should survive 7–10 h in jungle conditions, 5–7 weeks in ambient conditions, or 1.4–1.8 years in desert conditions. It is possible that other bonding methods and process conditions may be able to improve the moisture resistance and extend these durations.

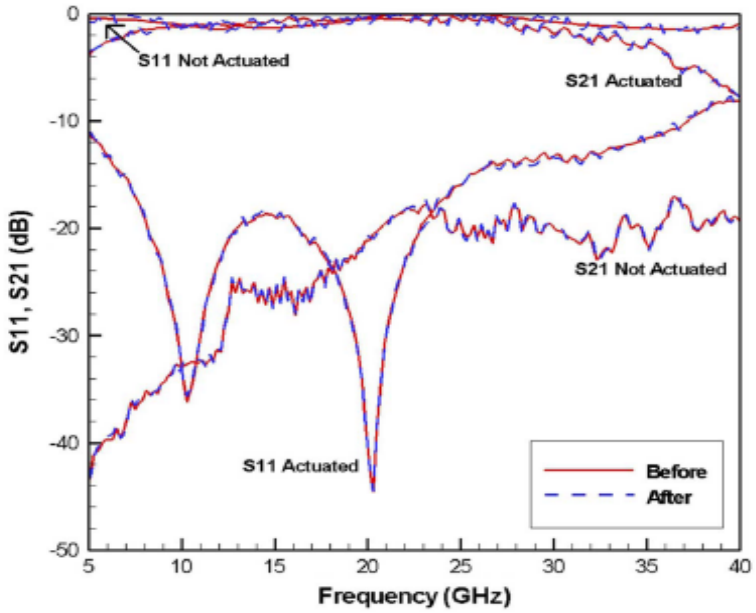

Fig. 27. S-parameter measurement results are shown for the working 30 min switch before and after moisture exposure. Less than 0.1 dB and 0.5 dB difference were measured between the S_{21} and S_{11} results, respectively. This is within the tolerance for measurement error.

E. High Gain Conformal Antenna on LCP Flexible Substrate

The 60 GHz unlicensed spectrum (56 GHz to 66 GHz) has received a lot of attention over the last couple of years for enabling over 1 Gbps high speed wireless communications. The propagation characteristics of this unlicensed frequency band is extreme because of the high atmospheric absorption (~10 dB/km at the sea level). These conditions require highly directive and high gain antennas at both the transmitter and the receiver to maximize the wireless communication throughput. End-Fire antennas [22]-[24] are very good candidates for such applications.

In this project, a linearly tapered slot antenna (LTSA) with a small form-factor ($2\lambda_0 \times \lambda_0$) is designed on liquid crystal polymer (LCP), - a flexible, light weight, low loss and low cost organic substrate [7]. Taking advantage of the LCP flexibility, the designed LTSA can conform to the surface

of commonly commercialized portable wireless devices. A prototype of the designed LTSA is fabricated and measured in both flat and conformed configurations.

E.1 Antenna design

The Linearly Tapered Slot Antenna (LTSA) is designed on an 8 mil thick LCP dielectric substrate (ε_r = 3.16, tan δ = 0.004 at 60 GHz [7]).The LTSA is patterned on the top side of the dielectric with a 3 um thick copper layer (Fig. 28a). The antenna is fed from the back, with a 50 Ω microstrip line patterned on the bottom side of the dielectric. The magnetic field surrounding the microstrip line couples easily to the magnetic field inside the slotline, such that a good microstrip-to-slotline transition is obtained [25]. The microstrip end is terminated with a circular stub for wider bandwidth characteristics [26]. The slot is tapered appropriately, such that the characteristic impedance of the slot at the open end is about 377 Ω, to provide good impedance matching and ensure proper radiation into the air. The overall antenna size is 10 mm × 5 mm (or $2\lambda_0 \times \lambda_0$ at 60 GHz). A detailed description of the antenna dimensions is given in Fig. 28b. Fig. 29 presents a photograph of the fabricated antenna on the LCP substrate.

E.2 Simulation and measurement results

Fig. 30 shows the simulated [27] and measured return loss of the flat LTSA. The two plots are in good agreement. In simulation, a resonance occurs at 61.6 GHz and the bandwidth is about 5 GHz. In the measurements, a resonance appears around 62 GHz and the bandwidth is about 5.6 GHz. The flat antenna peak gain increases with frequency in both simulation and measurement, as expected for TSAs (Fig. 31). The anomalous drop in the measured peak gain, at 64 GHz, is probably caused by a small measurement error. The measured peak gain varies between 9.22 dBi and 9.98 dBi, and is about 0.5 dB higher than the simulated one.

A comparison of the simulated and measured half-power beamwidth (3 dB BW) gives an explanation to this. As shown in Fig. 32, the measured E-plane 3 dB BW (resp. H plane) is about 5° (resp. 12°) less than the simulated one. As the measured beam is narrower than the simulated one, the measured peak gain gets higher. Fig. 32 also shows that the 3 dB BW decreases with frequency.

The E plane (Θ = 90°) normalized radiation pattern at 62 GHz is plotted in Fig. 33a. The antenna pattern is scanned from Φ = 0° to Φ = 180°, with Φ = 90° representing the end-fire direction. The second half of the radiation pattern is not measured because of the mechanical limitations of the measurement tool. The minor asymmetry in both simulated and measured patterns is caused by the feeding line. The side lobe at Φ = 170° is about 6 dB higher than in simulation. Again, as the measured beamwidth is less than the simulated one, some part of the energy is radiated in the direction of the side lobe. The measured cross-polarized level is at least 11.95 dB less than the peak gain compared to the simulated value of 16.67 dB.

Fig. 33b shows the normalized radiation pattern in the H plane (Φ = 90°). The antenna pattern is scanned from Θ = 0° to Θ = 180°, with Θ = 90° representing the end-fire direction. The measured pattern shows a null at Θ = 134° whereas the corresponding simulated null appears at Θ = 162°. The narrower measured beam explains the high side lobe (~1.26 dBi) at Θ = 160°. The measured cross-polarized level is at least 12.95 dB less than the peak gain compared to the simulated value of 20 dB.

The LTSA is finally conformed such as to have a curvature radius of 19 mm (Fig.1a). This step is carried out to evaluate the performance of the antenna when it is conformed to a curved surface for mobile platform insertion. The H plane pattern of the conformed antenna rotates by about 18° in the direction through which it is curved (Fig. 34). The conformed LTSA has a 7.48 dBi peak gain, that is, 2.5 dB less than the flat antenna. These observations indicate that wrapping the LTSA for mounting on a mobile platform plastic chassis will direct the beam toward the curving direction, with a slight peak gain drop.

We demonstrated an end-fire linearly tapered slot antenna with a very small form-factor ($2\lambda_0 \times \lambda_0$), a 5.6 GHz measured bandwidth and a 9.98 dBi measured peak gain, designed on LCP substrate for 60 GHz wireless applications. When this antenna is conformed to a curved surface, the beam is tilted toward the direction in which it is curved. Wrapping the LTSA also decreases the peak gain by about 2.5 dB. Overall, this conformal antenna exhibits very encouraging performance and should suit well for 60GHz wireless applications.

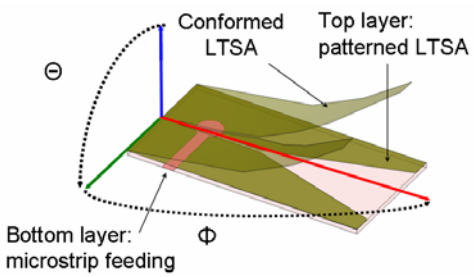

Fig. 28a. 3D view of the designed LTSA.

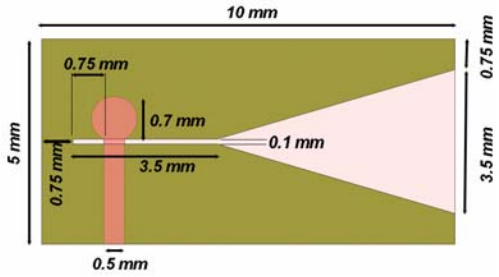

Fig. 28b. Top view of the LTSA.

Fig. 29. Photograph of the fabricated LTSA.

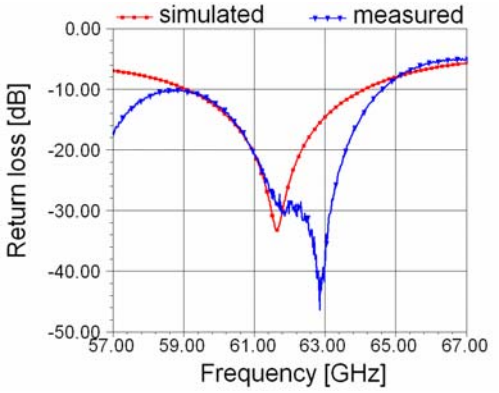

Fig. 30. Simulated and measured return loss of the flat LTSA.

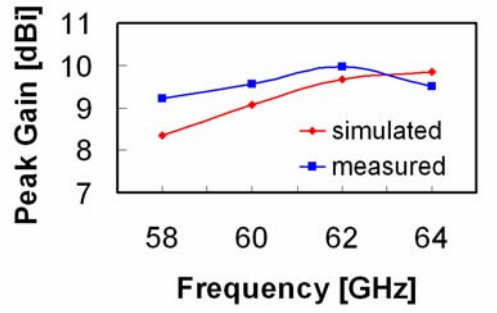

Fig. 31. Peak gain of the flat LTSA as a function of frequency.

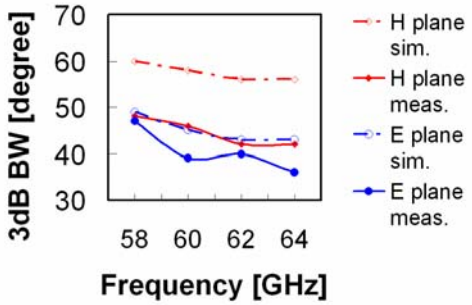

Fig. 32. Simulated and measured H and E-plane 3 dB BW of the flat LTSA.

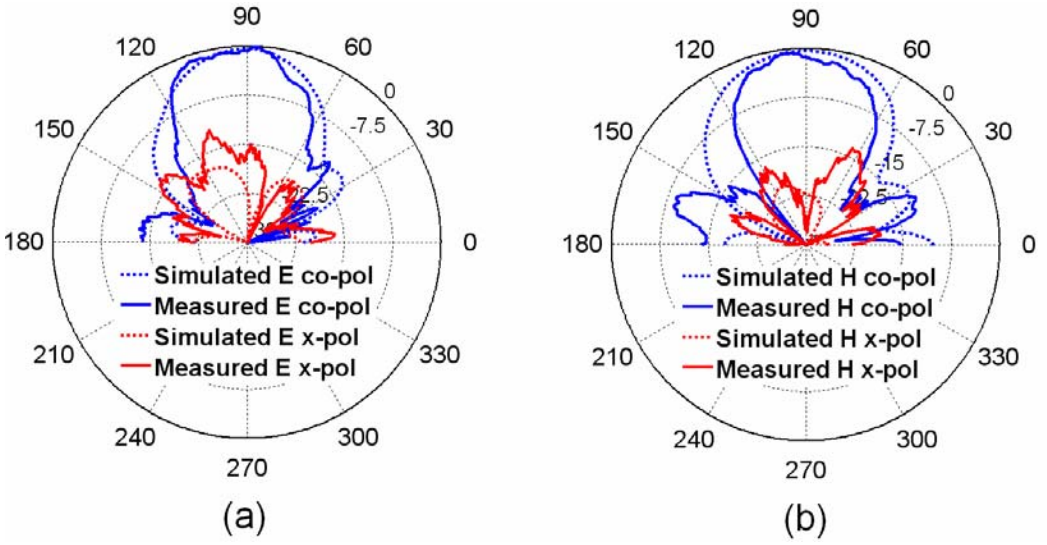

Fig. 33. Normalized radiation pattern of the flat LTSA at 62 GHz: (a) E-plane (b) H-plane.

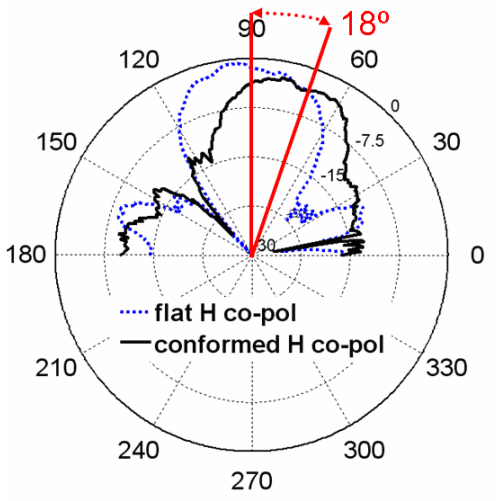

Fig. 34. Normalized H-plane patterns at 62 GHz: flat and conformed LTSA.

Publications and Products

Several journal and peer reviewed conference paper based on this research have been published. An invention disclosure has also been filed for the localized packaging MEMS switch technique. The latter has received strong interest from several companies that manufacture MEMS devices.

1) D. Anagnostou, R. Bairavasubramanian, G. DeJean, N. Kingsley, M. Tentzeris and J. Papapolymerou, "Development of a Dual-Frequency, Dual-Polarization Flexible and Deployable Antennas Array for Weather Applications," presented at the 15th IST Mobile & Wireless Communications Summit, Athens, Greece, June 2006.
2) M. Morton, N. Kingsley and J. Papapolymerou, "Low Cost Method for Localized Packaging of Temperature Sensitive Capacitive RF MEMS Switches in Liquid Crystal Polymer," *2007 IEEE International Microwave Symposium*, pp. 2075-2078, Honolulu, HI, June 2007.
3) N. Kingsley, D. Anagnostou, M. Tentzeris and J. Papapolymerou, "RF MEMS Sequentially-Reconfigurable Sierpinski Antenna on a Flexible, Organic Substrate without the Need for DC Bias Lines," *IEEE/ASME Journal of Microelectromechanical Systems*, Vol. 16, No. 5, pp. 1185-1192, October 2007.
4) N. Kingsley, S. Bhattacharya and J. Papapolymerou, "Moisture Lifetime Testing of RF MEMS Switches Packaged in Liquid Crystal Polymer," *IEEE Transactions on Components and Packaging Technologies,* Vol. 31, No. 2, pp. 345-350, June 2008.
5) T. Wojtaszek, J.T. Bernhard, G.H. Huff, D. Chung and J. Papapolymerou, "Reconfigurable Antennas with Integrated RF MEMS Switches for Military MIMO Applications," *presented at the 2009 COMAC Symposium*, March 2009.
6) Arnaud L. Amadjikpe, Debabani Choudhury, George E. Ponchak and John Papapolymerou, "A Compact Conformal End-Fire Antenna for 60 GHz Wireless Applications," *presented at the 2009 IEEE Antennas and Propagation International Symposium*, Charleston, SC, June 2009.
7) M. Morton, N. Kingsley, D. Thompson**,** M. Tentzeris and J. Papapolymerou, "Localized Bonding Technique for Near-Hermetic Packaging of RF MEMS Devices on Flexible, Organic substrate," submission of the invention for patent protection to U.S. Patent and Trademark Office on 10/10/2006 (provisional patent application-GTRC#3875).

Contributions

The activities that have been completed up to this point are the first steps for the development of a monolithic reconfigurable antenna system on organic, lightweight substrates that will enable portable MIMO systems. Our approach is a holistic one that keeps the goal – independent, uncorrelated channels achieved with minimal expense – in the foreground.

REFERENCES

[1] Nordquist, C.D. et al., "An X-band to Ku-band RF MEMS switched coplanar strip filter, "IEEE Microwave and Wireless Components Letters, Vol. 14, No. 9, pp. 425 - 427, Sept. 2004.
[2] Anagnostou, D.E. et al., "Design, fabrication, and measurements of an RF-MEMS-based self-similar reconfigurable antenna," IEEE Transactions on Antennas and Propagation, Vol. 54, No. 2, Part 1, pp. 422 - 432, Feb. 2006.
[3] Kingsley, N. and Papapolymerou, J., "Organic `Wafer-Scale' Packaged Miniature Four-Bit RF MEMS Phase Shifter", IEEE Transactions on Microwave Theory and Technique, Vol. 54, No. 3, March 2006.
[4] C. Puente, J. Romeu, R. Pous, A. Cardama, "On the behavior of the Sierpinski multiband fractal antenna", IEEE Transactions on Antennas and Propagation, vol. 46, no. 4, pages 517 - 524, April 1998.

[5] Kingsley, N., Wang, G., Papapolymerou, J., "Comparative Study of Analytical and Simulated Doubly-Supported RF MEMS Switches for Mechanical and Electrical Performance", Applied Computational Electromagnetics Society
Journal, Vol. 21, No. 1, pp. 9-15, March 2006.
[6] Comsol, Inc. "FEMLAB Multiphysics Modeling," http://www.comsol.com/products/femlab, November 2004.
[7] D.C. Thompson, O. Tantot, H. Jallageas, G.E. Ponchak, M.M. Tentzeris, J. Papapolymerou, "Characterization of liquid crystal polymer (LCP) material and transmission lines on LCP substrates from 30 to 110 GHz", IEEE Transactions on Microwave Theory and Techniques, vol. 52, no. 4, pages 1343-1352, April 2004.
[8] IE3D™ is a trademark of Zeland Software.
[9] G. Du, Y. Zhang, Y. Ma, X. Yang, B. Zhao, B. Liu, "ZnO thin films grown by plasma-assisted metal-organic vapor phase epitaxy", Proceedings of the Sixth Chinese Symposium Optoelectronics, pages 292 - 296, 12-14 Sept. 2003.
[10] D. E. Anagnostou, G. Zheng, M. Chryssomallis, J. Papapolymerou, C. G. Christodoulou, J. Lyke, G. Ponchak, "Design, Fabrication and Measurements of a Self-Similar Re-configurable Antenna with RF-MEMS Switches",
IEEE Transactions on Antennas & Propagation, Special Issue on Multifunction Antennas and Antenna Systems, vol. 54, no. 2, Feb 2006.
[11] S. Horst, S. Bhattacharya, S. Johnson, E. Tentzeris, and J. Papapolymerou, "Modeling and Characterization of Thin Film Broadband Resistors on LCP for RF Applications", Proc. 56th Electronic Components and Technology Conf., pg. 1751-1755, June 2006.
[12] D. Thompson, N. Kingsley, Guoan Wang; J. Papapolymerou, M.M. Tentzeris, "RF characteristics of thin film liquid crystal polymer (LCP) packages for RF MEMS and MMIC integration," Microwave Symposium Digest, 2005 IEEE MTT-S International, pp. 12-17, June 2005.
[13] R. Dean, J. Pack, N. Sanders, P. Reiner, "Micromachined LCP for packaging MEMS sensors," Industrial Electronics Society, 2005. IECON 2005. 32nd Annual Conference of IEEE, pp. 6-10, Nov. 2005.
[14] M. Chen, A. Pham, C. Kapusta, J. Iannotti, W. Kornrumpf, N. Evers,
J. Maciel, and N. Karabudak, "Development of Multilayer Organic Modules for Hermetic Packaging of RF MEMS Circuits," Microwave Symposium Digest, 2006 IEEE MTT-S International, pp. 271-274, June 2006.
[15] M. Chen, A. Pham, N.A. Evers, C. Kapusta, J. Iannotti, W. Kornrumpf,
N. Evers, J. Maciel, and N. Karabudak, "Design and Development of a Package Using LCP for RF/Microwave MEMS Switches," IEEE Trans. on Microwave Theory and Techniques, Vol 54, no 11, pp. 4009-4014, Nov 2006.
[16] Internet, http://www.radantmems.com/radantmems.data/Library/RadantDatasheetRMSW200.pdf, 2006.
[17] Personal communication with Dr. C. Goldsmith, President of Memtronics.
[18] Yu-Chuan Su, L. Lin, "Localized bonding processes for assembly and packaging of polymeric MEMS," IEEE Trans. on Packaging and Manufacturing., Vol. 28, Issue 4, pp. 635-642, Nov. 2005.
[19] Y. Cheng, L. Lin and K. Najafi, "A Hermetic Glass-Silicon Package Formed Using Localized Aluminum/Silicon-Glass Bonding," Journal of Microelectromechanical Systems, Vol. 10, no. 3, pp. 392-399, 2001.
[20] G. Wang, D. Thompson, M.M. Tentzeris, J. Papapolymerou, "Low cost RF MEMS switches using LCP substrate," in Proc. 34th Eur. Microw. Conf.,Oct. 2004, pp. 1-3.
[21] Comsol, Inc., "COMSOL Multiphysics Simulator", Internet, http://www.comsol.com, 2006.
[22] K. W. Kim, Y. Rahmat-Samii, "Handset antennas and humans at Ka-band: the importance of directional antennas," *IEEE Transactions on Antennas and Propagation,* Vol. 46, No. 6, pp. 949-950, June 1998.
[23] H. Oraizi, S. Jam, "Optimum Design of Tapered Slot Antenna Profile," *IEEE Transactions on Antennas and Propagation,* Vol. 51, No. 8, pp. 1987-1995, August 2003.
[24] R. Janaswamy, D. H. Schaubert, "Analysis of the Tapered Slot Antenna," *IEEE Transactions on Antennas and Propagation,* Vol. 35, No. 9, pp. 1058-1065, September 1987.
[26] K. C. Gupta, R. Garg, I. Bahl, P. Bhartia *Microstrip Lines and Slotlines* Nordwood, MA: Artech House, 1996, pp. 305.
[27] K. C. Gupta, R. Garg, I. Bahl, P. Bhartia *Microstrip Lines and Slotlines* Nordwood, MA: Artech House, 1996, pp. 312.
[28] http://www.ansoft.com/HFSS/